A Journal of the Gesellschaft Deutscher Chemiker

Angewandte International Edition GDCh Chemie

www.angewandte.org

Accepted Article

Title: Synergistic Metal-Nonmetal Active Sites in a Metal-Organic Cage for Efficient Photocatalytic Synthesis of Hydrogen Peroxide in Pure Water

Authors: Jia-Ni Lu, Jing-Jing Liu, Long-Zhang Dong, Jiao-Min Lin, Fei Yu, Jiang Liu, and Ya-Qian Lan

To be cited as: *Angew. Chem. Int. Ed.* **2023**, e202308505

Link to VoR: https://doi.org/10.1002/anie.202308505

WILEY VCH

10.1002/anie.202308505

WILEY VCH

RESEARCH ARTICLE

Synergistic Metal-Nonmetal Active Sites in a Metal-Organic Cage for Efficient Photocatalytic Synthesis of Hydrogen Peroxide in Pure Water

Jia-Ni Lu,[+a] Jing-Jing Liu,[+b] Long-Zhang Dong,[b] Jiao-Min Lin,[b] Fei Yu,[a] Jiang Liu,*[a,b] and Ya-Qian Lan*[a,b]

[a] J.-N. Lu, Prof. F. Yu, Prof. J. Liu, Prof. Y.-Q. Lan
Jiangsu Collaborative Innovation Centre of Biomedical Functional Materials, Jiangsu Key Laboratory of New Power Batteries, School of Chemistry and Materials Science
Nanjing Normal University
Nanjing, 210023, P. R. China
E-mail: liuj@njnu.edu.cn; liuj0828@m.scnu.edu.cn; E-mail: yqlan@m.scnu.edu.cn; yqlan@njnu.edu.cn

[b] J.-J. Liu, L.-Z. Dong, Prof. J.-M. Lin, Prof. J. Liu, Prof. Y.-Q. Lan
School of Chemistry
South China Normal University
Guangzhou, 510006, P. R. China

[+] These authors contributed equally to this work.

Abstract: Photocatalytic synthesis of hydrogen peroxide (H_2O_2) is a potential clean method, but the long distance between the oxidation and reduction sites in photocatalysts hinders the rapid transfer of photogenerated charges, limiting the improvement of its performance. Here, a metal-organic cage photocatalyst, **Co_{14}(L-CH_3)$_{24}$**, is constructed by directly coordinating metal sites (Co sites) used for O_2 reduction reaction (ORR) with non-metallic sites (imidazole sites of ligands) used for H_2O oxidation reaction (WOR), which shortens the transport path of photogenerated electrons and holes, and improves the transport efficiency of charges and activity of photocatalyst. Therefore, it can be used as an efficient photocatalyst with a rate of as high as 146.6 μmol g^{-1} h^{-1} for H_2O_2 production under O_2-saturated pure water without sacrificial agents. Significantly, the combination of photocatalytic experiments and theoretical calculations proves that the functionalized modification of ligands is more conducive to adsorbing key intermediates (*OH for WOR and *HOOH for ORR), resulting in better performance. This work proposed a new catalytic strategy for the first time, that is, to build a synergistic metal-nonmetal active site in the crystalline catalyst and use the host-guest chemistry inherent in MOC to increase the contact between the substrate and the catalytic active site, and finally achieve efficient photocatalytic H_2O_2 synthesis.

Introduction

As a clean chemical oxidant with only water and oxygen as byproducts, H_2O_2 is widely used in paper and textile bleaching, chemical synthesis, wastewater treatment, and small-scale fuel cells due to its low cost and minimal environmental impact.[1] At present, the anthraquinone process, electrocatalytic O_2 reduction, and direct synthesis by H_2 and O_2 are the main methods for producing H_2O_2.[2] However, these methods still have some disadvantages such as high energy consumption, high cost, and serious safety issues.[3] Therefore, people have been committed to develop environmentally friendly and low-cost ways to achieve efficient H_2O_2 production.[4] Photocatalytic synthesis of H_2O_2 is a potential green synthesis method, which combines the photocatalytic WOR and ORR under sunlight irradiation to prepare H_2O_2.[5] So far, the catalysts widely used in the photocatalytic H_2O_2 synthesis reaction are mainly inorganic semiconductors (such as TiO_2, $BiVO_4$, and CdS), g-C_3N_4-based photocatalysts, organic polymers and metal-organic complexes.[6] Most of them are composite materials, and their non-periodic structures make it relatively difficult to reveal the structure-activity relationship. On the contrary, constructing catalysts with well-defined periodic structures can solve this problem and establish accurate structure-activity relationships, which may in turn guide the design and synthesis of catalyst with improved performance.

Coordination compounds are crystalline materials formed by self-assembly of metal ions/clusters and organic ligands.[7] Its metal sites and nonmetal sites (the ligands) can be used as active sites of WOR and ORR, respectively. Through direct coordination of the two, the space distance between oxidation site and reduction site can be shortened, which is conducive to improving the separation efficiency of photogenerated electrons and holes, and thus enhancing the rate of photocatalytic H_2O_2 synthesis. Among them, metal organic cage (MOC),[8] as a kind of hollow polymetallic cluster, can not only achieve the synergy between the above-mentioned metal-nonmetal active sites through metal-ligand coordination, but also contain multiple metal active sites. Generally, in MOC, with the increase of its nucleus number, more active sites can be exposed, which is beneficial for improving the catalytic activity.[9] Moreover, they have a unique cavity structure, and the reaction molecules can usually enter the cavity easily.[10] Thus, the reaction molecules can attack the catalytic active site from both inside and outside of the cavity to make the reaction more fully.[11] More importantly, they have well-defined crystal structures,[12] which are beneficial for studying reaction

mechanisms and structure-activity relationships, and for optimizing and designing efficient photocatalysts.[13]

Based on the above considerations, we constructed two stable Co^{II}-based MOCs (**Co_{14}(L-H)$_{24}$** and **Co_{14}(L-CH_3)$_{24}$**) with the same main framework. Among them, **Co_{14}(L-CH_3)$_{24}$** is obtained by functionalizing the ligand of **Co_{14}(L-H)$_{24}$** with the -CH_3 group. Both types of supramolecular cages can serve as catalysts for the photocatalytic synthesis of H_2O_2 reaction. Due to the functionalization of MOCs, the light absorbance of the photocatalyst is improved, and the recombination efficiency of photogenerated electrons and holes is reduced. Moreover, theoretical calculations reveal that the -CH_3 functionalized ligand is more favorable to adsorb the key *OH and *HOOH intermediates generated by WOR and ORR. Therefore, **Co_{14}(L-CH_3)$_{24}$** exhibits a higher H_2O_2 generation rate of 146.60 μmol g^{-1} h^{-1}. Comparative experiments, isotope tracing experiments, and computational results jointly demonstrate that, for these two catalysts, the imidazole site from the ligand is the oxidation site, generating H_2O_2 through the $2e^-$ two-steps WOR pathway, while the Co site serves as the reduction site, enabling the synthesis of H_2O_2 through the $2e^-$ two-steps ORR route. More importantly, the imidazole site directly coordinates with the Co site in these Co^{II}-based supramolecular cages, narrowing the spatial distance between the oxidation and reduction sites, and improving the migration efficiency of charges, and thus improving the catalytic activity of photocatalytic H_2O_2 synthesis. This work is the first to construct a synergistic metal-nonmetallic active site for photocatalytic H_2O_2 synthesis reaction and the reaction substrate can more fully contact the catalytic active site through host-guest chemistry, ultimately achieving an efficient H_2O_2 production rate.

Results and Discussion

The HL-CH_3 ligand was obtained by functionalizing the benzene ring of the HL-H ligand with -CH_3 group. And they can assemble with Co metal ions to form Co^{II}-based metal-organic cages, **Co_{14}(L-H)$_{24}$** (Co_{14}(L-H)$_{24}$(H_2O)$_{12}$(NO_3)$_4$, HL-H = N-benzyl-1-(1H-imidazol-4-yl)methanimine) and **Co_{14}(L-CH_3)$_{24}$** (Co_{14}(L-CH_3)$_{24}$(H_2O)$_{12}$(NO_3)$_4$, HL-CH_3 = 1-(1H-imidazol-4yl)-N-(4-methylbenzyl)methanimine). Single crystal X-ray diffraction analysis reveals that **Co_{14}(L-H)$_{24}$** crystallizes in cubic space group *F23* with an asymmetric unit consisting of three cobalt ions, two L-H ligands, and two water molecules (Figure S5). Meanwhile, **Co_{14}(L-CH_3)$_{24}$** crystallizes in cubic space group *F432* with an asymmetric unit consisting of two cobalt ions, one L-CH_3 ligand, and two water molecules (Figure S6). **Co_{14}(L-H)$_{24}$** and **Co_{14}(L-CH_3)$_{24}$** share similar coordination methods. Co1 is coordinated with imidazole N of four L-H or L-CH_3 ligands and two water molecules to form an octahedral coordination structure (Figure 1b and Figure S7). Significantly, under external stimuli, two water molecules are easy to break away from the Co1 site to form the square coordinated Co site, which becomes the open catalytic active site. Co2 is a six-coordination site with six N atoms from three L-H or L-CH_3 ligands (Figure 1c and Figure S8). By means of the above connection, every cage of **Co_{14}(L-H)$_{24}$** (Figure 1a) and **Co_{14}(L-CH_3)$_{24}$** (Figure S10) is a rhombic dodecahedron cage containing fourteen Co atoms and twenty-four ligands. For **Co_{14}(L-H)$_{24}$** and **Co_{14}(L-CH_3)$_{24}$**, the cavity diameter of the cage is about 6.61 Å and 6.55 Å, respectively. If the water molecules of Co1 break away, the diameter of the cavity increases to 10.93 Å and 10.88 Å, respectively (Figure 1d-e). Reactive molecules such as H_2O and O_2 are easy to reach the cavity. Thus, they can attack the active site from both inside and outside the cavity, which is conducive to improving the catalytic activity.

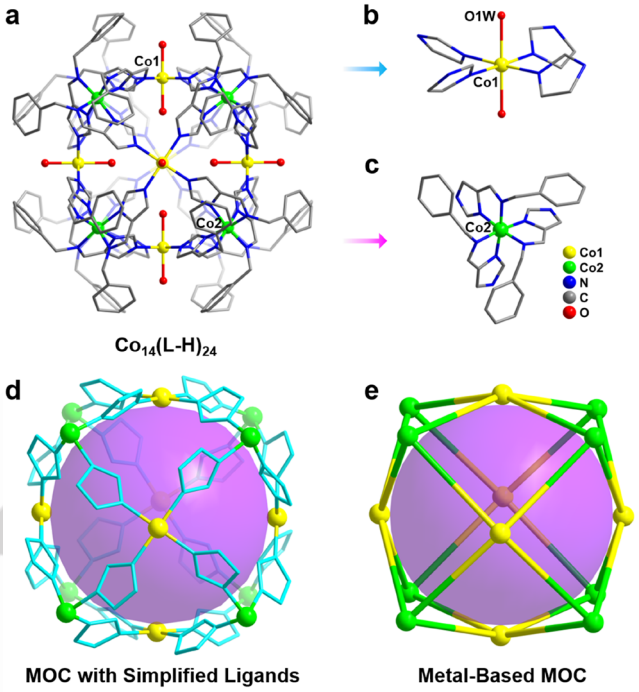

Figure 1. (a) The crystal structures of **Co_{14}(L-H)$_{24}$**. (b) The coordination environment of Co1 in **Co_{14}(L-H)$_{24}$**. (c) The coordination environment of Co2 in **Co_{14}(L-H)$_{24}$**. (d) The simplified structure of cage containing Co sites and imidazole sites. (e) The simplified structure of cage containing only Co sites.

The purity of **Co_{14}(L-H)$_{24}$** and **Co_{14}(L-CH_3)$_{24}$** was proved by the well-matched simulated and experimental powder X-ray diffraction (PXRD) patterns (Figure S12). The thermal stability of them was demonstrated by the thermogravimetric analyses, which showed that both MOCs could remain the structural stability until about 280 °C (Figures S13-S14). X-ray photoelectron spectroscopy (XPS) was tested to prove the elements contained in the crystals. The results revealed that both crystals contained Co, C, N and O elements (Figure S15). Moreover, the Co 2p of **Co_{14}(L-H)$_{24}$** contained Co $2p_{1/2}$ and Co $2p_{3/2}$ with binding energy of 796.15 and 781.24 eV, demonstrating the oxidation state of the Co ion was +2 (Figure S16). In addition, compared with **Co_{14}(L-H)$_{24}$**, the Co $2p_{1/2}$ (796.62 eV) and Co $2p_{3/2}$ (781.55 eV) of **Co_{14}(L-CH_3)$_{24}$** had the positive shift, which represented a reduction in the charge density of Co atom in **Co_{14}(L-CH_3)$_{24}$**.

Optical microscope imaging revealed that the morphology of **Co_{14}(L-H)$_{24}$** was orange polyhedral single crystal and **Co_{14}(L-CH_3)$_{24}$** was reddish brown polyhedral single crystal (Figure S17). Because of the different color of these compounds, we tested their

light absorption capacity by solid-state ultraviolet, visible and near-infrared diffuse reflectance spectroscopy (UV/Vis-NIR DRS). As shown in Figure 2a, **Co_{14}(L-CH_3)$_{24}$** had stronger light absorption capacity than **Co_{14}(L-H)$_{24}$** in a broad region from 300 to 1100 nm. Based on the Kubelka-Munk function, the optical band gap (E_g) of **Co_{14}(L-H)$_{24}$** and **Co_{14}(L-CH_3)$_{24}$** were estimated to be 2.12 eV and 1.95 eV (Figures S18-S19), respectively, revealing their potential to act as semiconducting photocatalysts. The lowest unoccupied molecular orbital (LUMO) positions of these semiconductor-like crystals were determined by Mott-Schottky measurements (Figures S20-S21). The final LUMO positions of crystals were calculated to be −0.18 V (vs normal hydrogen electrode, NHE, pH = 7) for **Co_{14}(L-H)$_{24}$** and −0.16 V (vs NHE, pH = 7) for **Co_{14}(L-CH_3)$_{24}$**. Therefore, the highest occupied molecular orbital (HOMO) positions of **Co_{14}(L-H)$_{24}$** and **Co_{14}(L-CH_3)$_{24}$** were calculated to be 1.94 and 1.79 V (vs NHE, pH = 7) through UV/Vis-NIR DRS and Mott-Schottky measurements. In addition, ultraviolet photoelectron spectroscopy (UPS, Figures S22-S23) was tested to calculate the HOMO positions to further verify the accuracy of the above results. By subtracting the excitation energy of 21.22 eV from the width of the He I UPS spectrum, the HOMO positions of **Co_{14}(L-H)$_{24}$** and **Co_{14}(L-CH_3)$_{24}$** were estimated to be −6.81 and −6.64 eV (vs. vacuum level, E_v), respectively. These results were well agreed with those calculated by UV/Vis-NIR DRS and Mott-Schottky measurements, demonstrating that the above test results were credible. The band structures of these photocatalysts were illustrated in Figure 2b. Obviously, the LUMO positions of these catalysts were more negative than the redox potential of O_2/H_2O_2 (0.68 V vs. NHE, pH = 7)[14], and the HOMO positions of them were more positive than the oxidation potential of H_2O/H_2O_2 (1.78 V vs. NHE, pH = 7).[15] Therefore, both crystals may have potential to act as photocatalysts for ORR and WOR toward H_2O_2 evolution. In addition, **Co_{14}(L-CH_3)$_{24}$** possesses a narrower band gap for capturing more photons, which may result in higher photocatalytic activity.

Electrochemical impedance spectroscopy (EIS) measurement was performed to study the impedance of these two materials. As shown in Figure 2c, **Co_{14}(L-CH_3)$_{24}$** had a smaller semicircular diameter of Nyquist curves than **Co_{14}(L-H)$_{24}$**, indicating that the modification of ligand could reduce the internal resistance of the materials, improve the electronic conductivity, and enhance the charge transfer. To explore the charge separation efficiency of **Co_{14}(L-H)$_{24}$** and **Co_{14}(L-CH_3)$_{24}$**, we tested their transient short-circuit photocurrent response capacities and steady-state photoluminescence (PL) emission spectra. Both of **Co_{14}(L-H)$_{24}$** and **Co_{14}(L-CH_3)$_{24}$** had strong photocurrent response capacities (Figure 2d). More importantly, the transient photocurrent response intensities of **Co_{14}(L-CH_3)$_{24}$** was about twice that of **Co_{14}(L-H)$_{24}$**, reflecting higher photoelectron transport efficiency. As the Figure 2e showed, compared with **Co_{14}(L-H)$_{24}$**, the emission intensity of **Co_{14}(L-CH_3)$_{24}$** was significantly quenched, suggesting that the CH_3-modified **Co_{14}(L-CH_3)$_{24}$** had higher efficient at trapping photoexcited electrons and suppressing recombination of photogenerated charges. Meanwhile, the Figure 2f showed that **Co_{14}(L-CH_3)$_{24}$** (20.49 ns) exhibited a shorter excited stated lifetime with respect to **Co_{14}(L-H)$_{24}$** (40.87 ns), providing a lower recombination and higher separation efficiency of photoinduced electron-hole pairs. Based on the above results, between **Co_{14}(L-H)$_{24}$** and **Co_{14}(L-CH_3)$_{24}$**, the surface of the CH_3-modified photocatalyst had a higher density of photogenerated charges, so **Co_{14}(L-CH_3)$_{24}$** might have a higher photocatalytic activity for ORR and WOR.

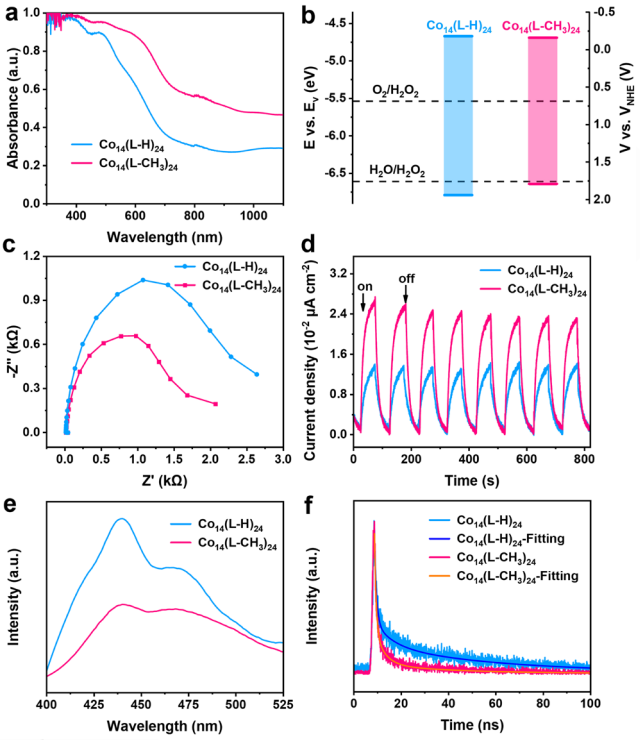

Figure 2. Characterizations of the optical properties for **Co_{14}(L-H)$_{24}$** and **Co_{14}(L-CH_3)$_{24}$**. (a) UV/Vis-NIR DRS spectra. (b) Band structure diagram. (c) EIS Nyquist plots. (d)Transient photocurrent response capacities. (e)The steady-state photoluminescence measurements. (f) Fluorescence decay curves.

The photocatalytic H_2O_2 production activities of the photocatalysts were carried out in O_2-saturated pure water without sacrificial agent, photosensitizer or pH adjustment under UV/Vis-NIR light (λ = 300-1100 nm). Figure 3a indicated that H_2O_2 production had a roughly linear relationship with reaction time. **Co_{14}(L-H)$_{24}$** showed a good catalytic activity with the H_2O_2 yield of 61.94 μmol g^{-1} over a period of 40 min. Interestingly, **Co_{14}(L-CH_3)$_{24}$** displayed higher photocatalytic activity. Under irradiation from 0 to 40 min, the H_2O_2 yield in the presence of **Co_{14}(L-CH_3)$_{24}$** was gradually increased and finally reached 97.73 μmol g^{-1}. It was worth noting that the H_2O_2 production rate for **Co_{14}(L-CH_3)$_{24}$** (146.60 μmol g^{-1} h^{-1}) was about 1.6 times that of **Co_{14}(L-H)$_{24}$** (92.91 μmol g^{-1} h^{-1}). More importantly, **Co_{14}(L-H)$_{24}$** and **Co_{14}(L-CH_3)$_{24}$** could photosynthesize H_2O_2 under air atmosphere, and their H_2O_2 production rates were 74.27 μmol g^{-1} h^{-1} and 120.04 μmol g^{-1} h^{-1}, respectively (Figure 3c). As far as we known, **Co_{14}(L-CH_3)$_{24}$** was the first metal-organic cage photocatalyst for H_2O_2 evolution in pure H_2O with O_2 or air atmosphere. In addition, the photocatalytic H_2O_2 synthesis rate was almost unchanged even after three cycling tests (Figure 3b), indicating that **Co_{14}(L-CH_3)$_{24}$**

10.1002/anie.202308505

were highly durable. Meanwhile, the PXRD (Figures S24-S25), FT-IR (Figures S26-S27), and XPS Co 2p spectra (Figures S28-S29) of **Co_{14}(L-H)$_{24}$** and **Co_{14}(L-CH_3)$_{24}$** obtained before and after photocatalytic tests showed similar structural features, further demonstrating the stability of these photocatalysts.

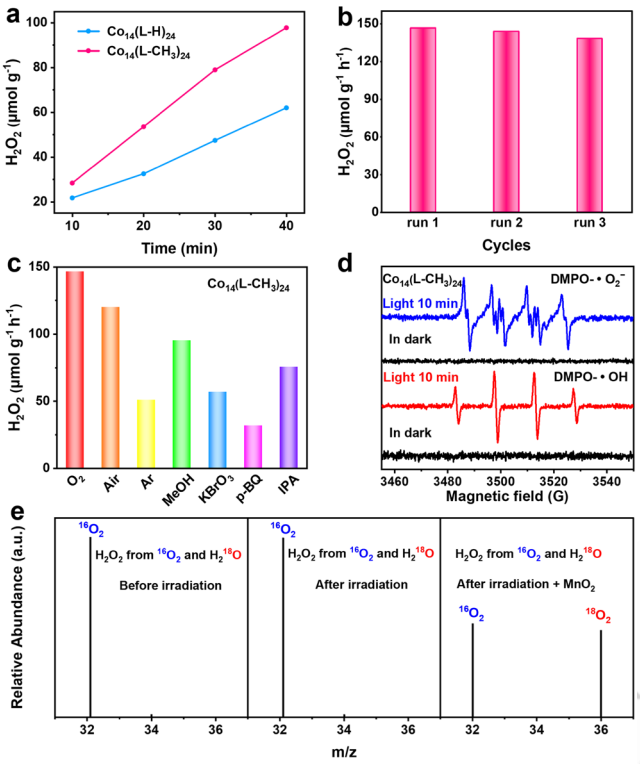

Figure 3. Performance of **Co_{14}(L-H)$_{24}$** and **Co_{14}(L-CH_3)$_{24}$** for photosynthesized H_2O_2. (a) Photocatalytic activity for H_2O_2 production in pure water and O_2 atmosphere. (b) Cycling performance. (c) Amounts of H_2O_2 produced in different conditions. (d) ESR signals of the reaction solution with **Co_{14}(L-CH_3)$_{24}$** under the dark and light illumination in the presence of DMPO as the spin-trapping reagents. (e) $H_2{}^{18}O$ isotope experiment to explore the source of H_2O_2 for **Co_{14}(L-CH_3)$_{24}$**.

In order to reveal the reaction pathways involved in H_2O_2 production, a series of control experiments was conducted (Figure 3c and Figure S30). Under the condition of Ar-saturated atmosphere, without O_2, a small amount of H_2O_2 was still produced under the catalysis of **Co_{14}(L-H)$_{24}$** and **Co_{14}(L-CH_3)$_{24}$**. In this case, the rates of H_2O_2 production were 36.51 μmol g^{-1} h^{-1} (**Co_{14}(L-H)$_{24}$**) and 50.77 μmol g^{-1} h^{-1} (**Co_{14}(L-CH_3)$_{24}$**), evidencing that both of them could catalyze water oxidation to produce H_2O_2. At the same time, the yield of H_2O_2 under Ar-saturated atmosphere was lower than that under O_2 atmosphere, which proved that H_2O_2 could be produced by ORR and WOR simultaneously in the presence of oxygen. We then looked into the two half-reaction (ORR and WOR) to find out the possible reaction pathways toward H_2O_2 evolution using **Co_{14}(L-H)$_{24}$** and **Co_{14}(L-CH_3)$_{24}$** as catalysts. For O_2 reduction half-reaction, H_2O_2 was continuously generated at a lower rate of 95.29 μmol g^{-1} h^{-1} for **Co_{14}(L-CH_3)$_{24}$** when MeOH was used as the hole acceptor. Similarly, when **Co_{14}(L-H)$_{24}$** acted as catalyst, the H_2O_2 production rate of ORR was decreased to 62.30 μmol g^{-1} h^{-1} with MeOH. This proved that both photocatalysts could reduce O_2 to H_2O_2. For H_2O oxidation half-reaction, with sufficient Ar bubbling to eliminate O_2 and $KBrO_3$ addition to act as the electron acceptor, no O_2 could be observed and a small amount H_2O_2 (23.52 μmol g^{-1} h^{-1} for **Co_{14}(L-H)$_{24}$** and 56.80 μmol g^{-1} h^{-1} for **Co_{14}(L-CH_3)$_{24}$**) was generated. These results revealed that H_2O was reactant and O_2 was not intermediate during photocatalytic WOR for the H_2O_2 production. So, **Co_{14}(L-H)$_{24}$** and **Co_{14}(L-CH_3)$_{24}$** underwent the 2e⁻ WOR process to produce H_2O_2.

$$O_2 + 2H^+ + 2e^- \rightarrow H_2O_2 \quad (1)$$

$$O_2 + e^- \rightarrow \bullet O_2^- \quad (2)$$

$$\bullet O_2^- + 2H^+ + e^- \rightarrow H_2O_2 \quad (3)$$

$$2H_2O + 2h^+ \rightarrow H_2O_2 + 2H^+ \quad (4)$$

$$H_2O + h^+ \rightarrow \bullet OH + H^+ \quad (5)$$

$$\bullet OH + \bullet OH \rightarrow H_2O_2 \quad (6)$$

According to the reported literature, there are two ORR pathways and two WOR routes for the 2-electron reaction of photocatalytic H_2O_2 synthesis in oxygen and pure water. For the ORR pathways, one is a 2e⁻ one-step reaction (equation 1), and the other is a 2e⁻ two-steps reaction with $\bullet O_2^-$ as intermediate (equations 2 and 3).[16] The WOR routes consist of a 2e⁻ one-step reaction (equation 4) and a 2e⁻ two-steps reaction with •OH as the intermediate species (equations 5 and 6).[17] In order to deeply explore the reaction pathways of WOR and ORR for **Co_{14}(L-H)$_{24}$** and **Co_{14}(L-CH_3)$_{24}$**, we analyzed the active species during the reaction process through trapping experiments. 1,4-benzoquinone (p-BQ) and isopropanol (IPA) were added to the photocatalytic H_2O_2 synthesis system as $\bullet O_2^-$ scavenger and •OH scavenger, respectively. Obviously, the produce rate of H_2O_2 decreased significantly. In the presence of p-BQ, the H_2O_2 production of **Co_{14}(L-H)$_{24}$** and **Co_{14}(L-CH_3)$_{24}$** decreased to 26.88 μmol g^{-1} h^{-1} and 31.76 μmol g^{-1} h^{-1}, respectively. This indicated that $\bullet O_2^-$ was necessary intermediate for the generation of H_2O_2 through ORR over both catalysts. Furthermore, electron spin resonance (ESR) was tested to verify this conclusion. As shown in Figure S31 and Figure 3d, no DMPO-$\bullet O_2^-$ signal of ESR was detected with the addition of the catalyst under dark conditions, while strong ESR DMPO-$\bullet O_2^-$ signals were detected when **Co_{14}(L-H)$_{24}$** and **Co_{14}(L-CH_3)$_{24}$** were catalyzed after 10 min of illumination. Therefore, $\bullet O_2^-$ was the critical intermediate of H_2O_2 production for **Co_{14}(L-H)$_{24}$** and **Co_{14}(L-CH_3)$_{24}$**, and both photocatalysts produced H_2O_2 by virtue of the oxygen reduction path of 2-electron two-steps transfer.

On the other hand, the decreases of H_2O_2 generation of about 37.88% and 48.55% were observed when IPA was added to the system with **Co_{14}(L-H)$_{24}$** or **Co_{14}(L-CH_3)$_{24}$** as photocatalysts. So, •OH was key active species during the H_2O_2 production process by WOR. In addition, DMPO-•OH signals were detected for **Co_{14}(L-H)$_{24}$** and **Co_{14}(L-CH_3)$_{24}$** during the measurement of ESR spectra with illumination (Figure S31 and Figure 3d), which was consistent with the result of the •OH trapping experiment. Thus, it clearly proved that the WOR routes of two catalysts were a 2e⁻ two-steps process for photocatalytic H_2O_2 synthesis with •OH as the intermediate species.

10.1002/anie.202308505

RESEARCH ARTICLE

In order to further explore the source of O element in product H_2O_2, isotopic labeling control experiments were conducted using **$Co_{14}(L\text{-}CH_3)_{24}$** as photocatalyst. Specifically, 5 mg **$Co_{14}(L\text{-}CH_3)_{24}$** was ultrasonically dispersed into 2 mL of $H_2{}^{18}O$, which was purged with $^{16}O_2$ for 30 minutes to remove O_2 from the environment. Gas chromatography-mass spectrometer (GC-MS) was used to analyze the oxygen in the reactor head space before and after illumination. As shown in Figure 3e, no matter before the reaction or after the photocatalysis, only $^{16}O_2$ existed in the reaction system, without additional $^{18}O_2$, which proved that no $^{18}O_2$ intermediates were produced in the process of $H_2{}^{18}O$ oxidation to H_2O_2. In other words, the WOR process of **$Co_{14}(L\text{-}CH_3)_{24}$** was not a $4e^-$ transfer process, but a $2e^-$ process, which was consistent with the above results of trapping experiment and ESR measurement. It was worth noting that the photosynthesized H_2O_2 decomposed by MnO_2 produced a product consisting of approximately 1:1 $^{16}O_2$ and $^{18}O_2$. These indicated that H_2O and O_2 were both raw materials for photocatalytic H_2O_2 synthesis, and the atomic utilization rate of H_2O_2 synthesized by WOR and ORR was close to 100%.

In order to study the active site of the photocatalysts for WOR and ORR, we used density functional theory (DFT) calculation to compare the Gibbs free energies for H_2O and O_2 molecules adsorption at different sites (benzene ring site, C=N site, Co site, imidazole site) in **$Co_{14}(L\text{-}H)_{24}$** and **$Co_{14}(L\text{-}CH_3)_{24}$**. As shown in Figures S32-S33, the order of adsorption energies for H_2O at different sites in **$Co_{14}(L\text{-}H)_{24}$** and **$Co_{14}(L\text{-}CH_3)_{24}$** was imidazole site < benzene ring site < C=N site < Co site. More importantly, the imidazole sites of both catalysts had the same H_2O adsorption energies of −1.18 eV, indicating that the imidazole sites in both photocatalysts were active sites for H_2O oxidation reaction. To verify this conclusion, we tested the performance of ligands (L-H and L-CH_3) as photocatalysts for the photocatalytic H_2O_2 synthesis reaction. As shown in Figure S34, in pure water saturated with O_2, the rates of generating H_2O_2 for L-H and L-CH_3 were 18.53 μmol g^{-1} h^{-1} and 24.31 μmol g^{-1} h^{-1}, respectively. When $KBrO_3$ was added as the hole acceptor to test the half-reaction of H_2O oxidation, the synthesis rates of H_2O_2 had significantly increased, reaching 35.73 μmol g^{-1} h^{-1} and 50.09 μmol g^{-1} h^{-1}, respectively. The increase in rate in the presence of $KBrO_3$ indicated that the production of H_2O_2 might not occur through photo-induced electron via O_2 reduction reaction, as these photogenerated electrons were consumed by the hole donors. This result proved that pure ligands (L-H and L-CH_3) could catalyze WOR to generate H_2O_2, and electron trapping agents promoted the interaction between holes and catalysts, improving the photocatalytic efficiency. Therefore, the active sites where these Co-based supramolecular catalysts underwent WOR were in their ligand segments.

However, the order of adsorption energies for O_2 at these sites of **$Co_{14}(L\text{-}H)_{24}$** and **$Co_{14}(L\text{-}CH_3)_{24}$** was different (Figures S35-S36). In **$Co_{14}(L\text{-}H)_{24}$**, the order of O_2 adsorption energy was exactly opposite to that of H_2O adsorption energy, which was imidazole site > benzene ring site > C=N site > Co site. At the same time, the adsorption energies for O_2 at C=N site, imidazole site, benzene ring site, and Co site of **$Co_{14}(L\text{-}CH_3)_{24}$** gradually decreased, which were −0.45 eV, −0.65 eV, −1.04 eV, and −1.77 eV, respectively. It is worth noting that the Co sites of **$Co_{14}(L\text{-}H)_{24}$** and **$Co_{14}(L\text{-}CH_3)_{24}$** had the similar lowest adsorption energies for O_2 of −1.76 eV and −1.77 eV, respectively. Therefore, the catalytic active site for O_2 reduction reaction was the Co site. It is worth noting that Co2 is fully coordinated, and the two coordinated water molecules of Co1 are easy to leave to form the active site, so the reduction site of catalytic ORR is the Co1 site.

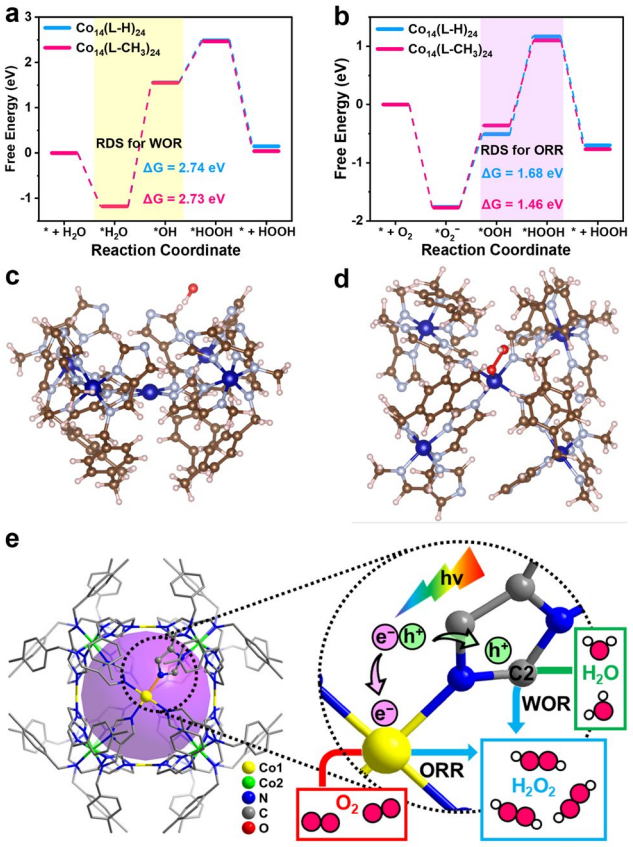

Figure 4. Free energy diagram of the **$Co_{14}(L\text{-}H)_{24}$** and **$Co_{14}(L\text{-}CH_3)_{24}$** for photosynthesize of H_2O_2 through the (a) WOR and (b) ORR pathways. (c) Adsorption configuration of $^*OH$ intermediates on C2−H of the imidazole sites in **$Co_{14}(L\text{-}CH_3)_{24}$**. (d) Adsorption configuration of $^*OOH$ intermediates on Co sites in **$Co_{14}(L\text{-}CH_3)_{24}$**. (e) The proposed reaction mechanism for photosynthesized of H_2O_2.

In order to further reveal the influence of ligand modification on H_2O oxidation reaction and O_2 reduction reaction, we calculated the free energies of each step in the two reaction pathways. As shown in Figure 4a, the process of WOR was as follows: first, C2-H of the imidazole site adsorbed and activated H_2O molecules (Figure S37)[18], then H_2O decomposed to generate $^*OH$ intermediates. Figure 4c and Figure S38a showed that **$Co_{14}(L\text{-}H)_{24}$** and **$Co_{14}(L\text{-}CH_3)_{24}$** adsorbed $^*OH$ on C2−H of the imidazole sites. The next step was to combine two $^*OH$ to obtain $^*HOOH$, and finally, HOOH desorbed to produce H_2O_2. Obviously, the rate determining step (RDS) was to generate $^*OH$, and the free energy activation energy barriers (ΔG) of **$Co_{14}(L\text{-}H)_{24}$** and **$Co_{14}(L\text{-}CH_3)_{24}$** in this step were 2.74 eV and 2.73 eV, respectively.

Although the activation energy barriers of RDS for the two catalysts were similar, almost every step energy barrier of **Co_{14}(L-CH_3)$_{24}$** in the reaction path was slightly lower than that of **Co_{14}(L-H)$_{24}$**. Therefore, **Co_{14}(L-CH_3)$_{24}$** modified with -CH_3 had higher catalytic activity for WOR.

As shown in Figure 4b, the process of ORR was as follows: first, the Co site adsorbed and activated O_2 molecules to generate $^*O_2^-$, then $^*O_2^-$ combined with protons in the solution to generate *OOH intermediate and *HOOH intermediate, and finally desorbed to obtain H_2O_2. Figure 4d and Figure S38b displayed that **Co_{14}(L-H)$_{24}$** and **Co_{14}(L-CH_3)$_{24}$** adsorbed *OOH on Co sites. And the step of generating *HOOH from *OOH was the RDS in the O_2 reduction reaction in this reaction system. And the free energy barriers of **Co_{14}(L-H)$_{24}$** and **Co_{14}(L-CH_3)$_{24}$** in this step were 1.68 eV and 1.46 eV, respectively. Therefore, the -CH_3 modification on the ligand greatly reduced the energy barrier of the O_2 reduction reaction and improved the catalytic activity. Combining WOR and ORR, **Co_{14}(L-CH_3)$_{24}$** exhibited an overall lower free energy barrier, which was consistent with the higher H_2O_2 production rate obtained from experimental testing.

Based on experiments and calculations, we inferred the possible mechanism of Co-based supramolecular cages catalyzed photocatalytic synthesis of H_2O_2 (Figure 4e). Under light irradiation, photocatalysts absorbed light energy to generate photogenerated charges. Photogenerated electrons migrated to the Co site, causing the O_2 molecules adsorbed on the Co site to be reduced and underwent a proton/electron reaction process to gradually produce $^*O_2^-$, *OOH, and *HOOH. At the same time, C2−H of the imidazole sites absorbed and activated H_2O molecules through hydrogen-bonding-type interactions. Then, the transfer of photogenerated holes to the imidazole sites leaded to the oxidation of H_2O molecules adsorbed at this site, gradually generating *OH and *HOOH. Finally, *HOOH desorbed from the Co and imidazole sites to obtain H_2O_2. In MOCs, the imidazole sites and Co site coordinates directly, shortening the spatial distance between the oxidation sites and reduction sites, effectively improving the separation efficiency and migration rate of photogenerated charges, making it easier for H_2O to use holes and O_2 to capture electrons to form active intermediates, ultimately forming H_2O_2.

Conclusion

In summary, we obtained two stable metal-organic cages, **Co_{14}(L-H)$_{24}$** and **Co_{14}(L-CH_3)$_{24}$** by functionalizing the ligand with -CH_3 group. They could serve as difunctional photocatalysts, simultaneously catalyzing the H_2O oxidation reaction and the O_2 reduction reaction to synthesize H_2O_2. Because the ligand modification of -CH_3 increases the light absorbance of the photocatalyst and reduces the recombination efficiency of photogenerated charges, **Co_{14}(L-CH_3)$_{24}$** has higher catalytic activity for producing H_2O_2 in pure water. Under O_2 or air atmosphere, the H_2O_2 generation rates of **Co_{14}(L-CH_3)$_{24}$** are 146.60 μmol g^{-1} h^{-1} and 120.04 μmol g^{-1} h^{-1}, respectively. The experimental and computational results prove that the Co site and imidazole site catalyze 2e$^-$ two-steps O_2 reduction reaction and 2e$^-$ two-steps H_2O oxidation reaction, respectively. This work proved for the first time the great potential of metal-organic cages as photocatalysts in the field of H_2O_2 synthesis owing to its host-guest chemistry, and effectively improved the performance of photocatalytic H_2O_2 synthesis by virtue of its unique metal-nonmetal active sites synergistic catalysis.

Acknowledgements

This work was financially supported by NSFC (Nos. 92061101, 22271104, 21871141, and 22225109), the Excellent Youth Foundation of Jiangsu Scientific Committee (BK20211593), the project funded by China Postdoctoral Science Foundation (2018M630572), the Priority Academic Program Development of Jiangsu Higher Education Institutions, and the Foundation of Jiangsu Collaborative Innovation Center of Biomedical Functional Materials.

Conflict of Interest

The authors declare no conflict of interest.

Keywords: metal-organic cages • synergistic catalysis • host-guest chemistry • photocatalytic H_2O_2 synthesis • full reaction

References

[1] a) A. Gopakumar, P. Ren, J. Chen, B. V. Manzolli Rodrigues, H. Y. Vincent Ching, A. Jaworski, S. V. Doorslaer, A. Rokicińska, P. Kuśtrowski, G. Barcaro, S. Monti, A. Slabon, S. Das, *J. Am. Chem. Soc.* **2022**, *144*, 2603-2613; b) Y. Kofuji, S. Ohkita, Y. Shiraishi, H. Sakamoto, S. Tanaka, S. Ichikawa, T. Hirai, *ACS Catal.* **2016**, *6*, 7021-7029; c) B. He, Z. Wang, P. Xiao, T. Chen, J. Yu, L. Zhang, *Adv. Mater.* **2022**, *34*, 2203225; d) L. Xu, Y. Liu, L. Li, Z. Hu, J. C. Yu, *ACS Catal.* **2021**, *11*, 14480-14488; e) Z. Teng, Q. Zhang, H. Yang, K. Kato, W. Yang, Y.-R. Lu, S. Liu, C. Wang, A. Yamakata, C. Su, B. Liu, T. Ohno, *Nat. Catal.* **2021**, *4*, 374-384.

[2] a) L. Zhou, J. Lei, F. Wang, L. Wang, M. R. Hoffmann, Y. Liu, S.-I. In, J. Zhang, *Appl. Catal. B* **2021**, *288*, 119993; b) C. Krishnaraj, H. Sekhar Jena, L. Bourda, A. Laemont, P. Pachfule, J. Roeser, C. V. Chandran, S. Borgmans, S. M. J. Rogge, K. Leus, C. V. Stevens, J. A. Martens, V. Van Speybroeck, E. Breynaert, A. Thomas, P. Van Der Voort, *J. Am. Chem. Soc.* **2020**, *142*, 20107-20116; c) T. Ricciardulli, S. Gorthy, J. S. Adams, C. Thompson, A. M. Karim, M. Neurock, D. W. Flaherty, *J. Am. Chem. Soc.* **2021**, *143*, 5445-5464; d) M. Wang, X. Dong, Z. Meng, Z. Hu, Y.-G. Lin, C.-K. Peng, H. Wang, C.-W. Pao, S. Ding, Y. Li, Q. Shao, X. Huang, *Angew. Chem. Int. Ed.* **2021**, *60*, 11190-11195.

[3] a) J. Cai, J. Huang, S. Wang, J. Iocozzia, Z. Sun, J. Sun, Y. Yang, Y. Lai, Z. Lin, *Adv. Mater.* **2019**, *31*, 1806314; b) Y. Hong, Y. Cho, E. M. Go, P. Sharma, H. Cho, B. Lee, S. M. Lee, S. O. Park, M. Ko, S. K. Kwak, C. Yang, J.-W. Jang, *Chem. Eng. J.* **2021**, *418*, 129346; c) J. Luo, X. Wei, Y. Qiao, C. Wu, L. Li, L. Chen, J. Shi, *Adv. Mater.* **2023**, *35*, 2210110.

[4] a) Y. Zhao, Y. Liu, Z. Wang, Y. Ma, Y. Zhou, X. Shi, Q. Wu, X. Wang, M. Shao, H. Huang, Y. Liu, Z. Kang, *Appl. Catal. B* **2021**, *289*, 120035; b) B. Liu, J. Du, G. Ke, B. Jia, Y. Huang, H. He, Y. Zhou, Z. Zou, *Adv. Funct. Mater.* **2022**, *32*, 2111125.

[5] a) T. Liu, Z. Pan, J. J. M. Vequizo, K. Kato, B. Wu, A. Yamakata, K. Katayama, B. Chen, C. Chu, K. Domen, *Nat. Commun.* **2022**, *13*, 1034;

b) Y.-X. Ye, C. Wen, J. Pan, J.-W. Wang, Y.-J. Tong, S. Wei, Z. Ke, L. Jiang, F. Zhu, N. Zhou, M. Zhou, J. Xu, G. Ouyang, *Appl. Catal. B* **2021**, *285*, 119726.

[6] a) C. Liu, T. Bao, L. Yuan, C. Zhang, J. Wang, J. Wan, C. Yu, *Adv. Funct. Mater.* **2022**, *32*, 2111404; b) Y. Isaka, Y. Kawase, Y. Kuwahara, K. Mori, H. Yamashita, *Angew. Chem. Int. Ed.* **2019**, *58*, 5402-5406; c) E. Zhang, Q. Zhu, J. Huang, J. Liu, G. Tan, C. Sun, T. Li, S. Liu, Y. Li, H. Wang, X. Wan, Z. Wen, F. Fan, J. Zhang, K. Ariga, *Appl. Catal. B* **2021**, *293*, 120213; d) Y. Shiraishi, T. Takii, T. Hagi, S. Mori, Y. Kofuji, Y. Kitagawa, S. Tanaka, S. Ichikawa, T. Hirai, *Nat. Mater.* **2019**, *18*, 985-993; e) K. Kim, J. Park, H. Kim, G. Y. Jung, M.-G. Kim, *ACS Catal.* **2019**, *9*, 9206-9211.

[7] a) Y. Kondo, Y. Kuwahara, K. Mori, H. Yamashita, *Chem* **2022**, *8*, 2924-2938; b) K. Wang, Y. Li, L.-H. Xie, X. Li, J.-R. Li, *Chem. Soc. Rev.* **2022**, *51*, 6417-6441; c) Z. Chen, P. Li, R. Anderson, X. Wang, X. Zhang, L. Robison, L. R. Redfern, S. Moribe, T. Islamoglu, D. A. Gomez-Gualdron, T. Yildirim, J. F. Stoddart, O. K. Farha, *Science* **2020**, *368*, 297-303.

[8] a) X.-W. Zhu, D. Luo, X.-P. Zhou, D. Li, *Coord. Chem. Rev.* **2022**, *455*, 214354; b) G. Liu, M. Zhou, K. Su, R. Babarao, D. Yuan, M. Hong, *CCS Chem.* **2021**, *3*, 1382-1390; c) N. Takeda, K. Umemoto, K. Yamaguchi, M. Fujita, *Nature* **1999**, *398*, 794-796.

[9] J.-J. Liu, S.-N. Sun, J. Liu, Y. Kuang, J.-W. Shi, L.-Z. Dong, N. Li, J.-N. Lu, J.-M. Lin, S.-L. Li, Y.-Q. Lan, *J. Am. Chem. Soc.* **2023**, *145*, 6112-6122.

[10] S. Chen, K. Li, F. Zhao, L. Zhang, M. Pan, Y.-Z. Fan, J. Guo, J. Shi, C.-Y. Su, *Nat. Commun.* **2016**, *7*, 13169.

[11] a) Y. Xue, X. Hang, J. Ding, B. Li, R. Zhu, H. Pang, Q. Xu, *Coord. Chem. Rev.* **2021**, *430*, 213656; b) Y. Lu, H. Zhang, Y. Zhu, P. J. Marriott, H. Wang, *Adv. Funct. Mater.* **2021**, *31*, 2101335.

[12] P. Mal, B. Breiner, K. Rissanen, J. R. Nitschke, *Science* **2009**, *324*, 1697-1699.

[13] C. M. Hong, M. Morimoto, E. A. Kapustin, N. Alzakhem, R. G. Bergman, K. N. Raymond, F. D. Toste, *J. Am. Chem. Soc.* **2018**, *140*, 6591-6595.

[14] Y.-X. Ye, J. Pan, F. Xie, L. Gong, S. Huang, Z. Ke, F. Zhu, J. Xu, G. Ouyang, *P. Natl. Acad. Sci.* **2021**, *118*, e2103964118.

[15] L. Chen, L. Wang, Y. Wan, Y. Zhang, Z. Qi, X. Wu, H. Xu, *Adv. Mater.* **2020**, *32*, 1904433.

[16] Z. Chen, D. Yao, C. Chu, S. Mao, *Chem. Eng. J.* **2023**, *451*, 138489.

[17] M. Kou, Y. Wang, Y. Xu, L. Ye, Y. Huang, B. Jia, H. Li, J. Ren, Y. Deng, J. Chen, Y. Zhou, K. Lei, L. Wang, W. Liu, H. Huang, T. Ma, *Angew. Chem. Int. Ed.* **2022**, *61*, e202200413.

[18] S. Sung, X. Li, L. M. Wolf, J. R. Meeder, N. S. Bhuvanesh, K. A. Grice, J. A. Panetier, M. Nippe, *J. Am. Chem. Soc.* **2019**, *141*, 6569-6582.

10.1002/anie.202308505

WILEY VCH

RESEARCH ARTICLE

Entry for the Table of Contents

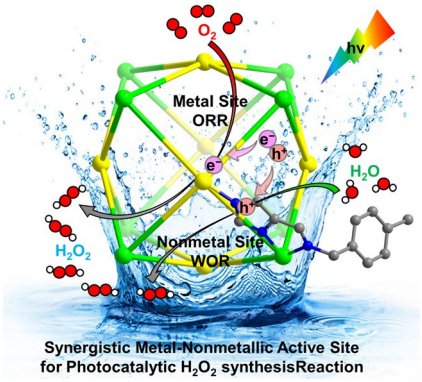

Two stable Co^{II}-based metal-organic cages are efficient catalysts for photocatalytic synthesis of H_2O_2 in pure water and O_2 or air atmospheres. The metal-nonmetal active site operates synergistically during photocatalytic H_2O_2 synthesis and the reaction substrate can more fully contact the catalytically active site through host-guest chemistry of cages, ultimately achieving a high H_2O_2 production rate.